The Deep Roots of Geology: Tectonic History of Australia and its Margins expressed by Mantle Anisotropy

Caroline Eakin (Caroline.Eakin@anu.edu.au)
Australian National University https://orcid.org/0000-0001-9187-3138

Research Article

Keywords: Australia, Quasi-Love waves, anisotropy

Posted Date: July 1st, 2021

DOI: https://doi.org/10.21203/rs.3.rs-121788/v2

Version of Record: A version of this preprint was published at Communications Earth & Environment on October 4th, 2021. See the published version at https://doi.org/10.1038/s43247-021-00276-7.

The Deep Roots of Geology: Tectonic History of Australia and its Margins expressed by Mantle Anisotropy

Caroline M. Eakin[1*]

[1]*Research School of Earth Sciences, Australian National University, Canberra, Australia*

Abstract

The Australian continental crust preserves a rich geological history, but it is unclear to what extent this history is expressed deeper within the mantle. Scattering of surface waves predominantly between 100-200 km depth by lateral gradients in seismic anisotropy, termed Quasi-Love waves, offer potential new insights. Across Australasia over 275 new scatterers are detected, and are found to be preferentially located near (1) the passive continental margins, and (2) the boundaries of major geological provinces within Australia. Such lateral anisotropic gradients imply pervasive fossilized lithospheric anisotropy within the continental interior, on a scale that mirrors the crustal geology at the surface, and a strong lithosphere that preserves this signal over billions of years. Along the continental margins, lateral anisotropic gradients may indicate either the edge of the thick continental lithosphere, or small-scale dynamic processes in the asthenosphere, such as edge-drive convection, tied to the transition from oceanic to continental lithosphere.

Introduction

The Australian continent preserves a vast tectonic history, stretching from the Archean to the present day [1,2]. By the Neoproterozoic, supercontinent cycles had assembled the three major Australian cratons (North, South, and West), while later continental accretion added the eastern orogens in the Phanerozoic [3]. Since the break-up of eastern Gondwana, and the formation of its rifted passive margins, the Australian continent has moved northwards colliding with SE Asia [4,5]. Today, Australia is the fastest moving continent on Earth [6], exerting significant shear on the underlying mantle asthenosphere. Such deformation is thought to cause a lattice preferred orientation (LPO) in olivine generating strong azimuthal anisotropy aligned with plate motion [7,8]. Intriguingly, this strong azimuthal anisotropy is not detected by shear-wave splitting studies, with weak and complex splitting generally observed across Australia [9–11]. Instead a contrasting contribution from fossilized anisotropy in the lithosphere has been proposed, frozen-in by past deformational events [10,12].

Observations of Love-to-Rayleigh surface wave scattering, termed Quasi-Love (QL) waves [13], can be used to pinpoint the location of lateral gradients in seismic anisotropy in the upper mantle (Fig. 1), such as those that may exist along present (and/or past) plate boundaries. When a Love wave encounters such a boundary, a portion of its energy is scattered from Love into Rayleigh wave motion, generating a QL wave (Fig. 1). The QL wave retains a similar waveform shape as the fundamental Love wave (G1), hence ‘Quasi-Love’, but travels with the slower velocity of the fundamental Rayleigh wave (R1). This principle can be exploited to determine the distance (δx) the QL wave has travelled and thus estimate the location of the anisotropic gradient. An anisotropic medium may also cause a small rotation of surface wave polarization [14–16]. These polarization-distortions are sometimes referred to in the literature as

42 'quasi-Love waves' also [17], however their characteristics are distinguishable from QL wave
43 scattering as described here (see Methods for further details). Previously QL wave scattering has
44 been detected across a wide range of tectonic settings from continental collision [18,19], seafloor
45 spreading [20], subduction [13,21–23], hotspot volcanism [24,25], and former continental rift zones [26].
46 Most recently QL waves have been recorded along the continental margin of eastern North
47 America [27], implying localized dynamic processes and a disruption of the underlying mantle
48 flow-field at the margin, potentially induced by the transition from continental to oceanic
49 lithosphere. As of yet, however, there have been no such studies targeting the rich history of the
50 Australian continent and its extensive passive margins.
51
52 **Results**
53 Using seismic stations from the Australian National Seismograph Network, and shallow
54 earthquakes (<50 km depth) at 70°-180° epicentral distances, robust QL wave detections were
55 measured on 22% of the 2248 available event-station pairs (Fig. 2, Supplementary Data Table
56 S1) with 276 QL scatterers falling within the study area, as shown in Fig. 3. The QL waves
57 detected are of varying amplitude (represented in Fig. 3 by their symbol size) which is not only a
58 function of the strength of the anisotropic gradient but also the geometry of the anisotropy
59 relative to the angle of the raypath. The back-projected scatterers are widely distributed,
60 comprising one of the largest and most geographically diverse QL datasets produced to date, as
61 well as the first results within Australasia. While the QL scatterers are widespread and numerous
62 (the reliability of any single measurement should be treated with caution), when considered
63 collectively, they display intriguing relationships with certain tectonic features at the Earth's
64 surface (Figs. 3-4 and Figs. S4-S11). Most noteworthy is the continental margins (cyan symbols;

Fig. 3a-b), that define the boundary between continental and oceanic crust [28]. Almost half of the scatterers (47%) fall within 200 km of this boundary. This is higher than expected considering just under two-fifths (38%) of the study area falls within 200 km (Fig. 4). The pattern is particularly intriguing around the Tasman Sea, along the former rift boundary between Australia and Te Riu-a-Māui/Zealandia (Fig. 3b). The scatterers appear to closely follow curvatures in this boundary and even coincide with micro-continents such as the East Tasman Plateau (ETP) and Gilbert Seamount Complex (GSC), which were isolated from the mainland during the rifting process [29].

The statistical significance of such a relationship between the location of scatterers and the ocean-continent boundary can be explored further. Fig. 4a shows the cumulative distribution function (CDF) of the minimum distance between each scatterer and the ocean-continent boundary (cyan line). This is compared with the average CDF (solid black curve) for 100 distributions (thin grey lines) of 276 randomly located points across the study area, the same as the number of QL scatterers in the dataset. The comparison indicates that there are more QL scatterers closer to the ocean-continent boundary than seen in the averaged properties of the 100 random distributions (i.e. the cyan curve is above the upper dashed black curve out to a distance of ~600 km). A two-sample Kolmogorov–Smirnov test [30–32] is performed to test the null hypothesis that the two CDFs are from the same continuous distribution. A p-value of 0.04 is found, suggesting that the null hypothesis can be rejected at 4% significance level, indicating that the QL scatterers can indeed be distinguished from a random distribution. Furthermore, sub-dividing the dataset into oceanic versus continental scatterers (Fig. S10) indicates that the spatial correlation is even stronger within the oceans (p value = 0.01), with 38% of the oceanic

scatterers located within 100 km of the ocean-continent boundary, which is more than 2.5 standard deviations higher than the mean of the random distributions.

Away from the continental margins, scatterers can also be found within the Australian continental interior coinciding with the boundaries between major geological provinces[33] (yellow symbols; Fig. 3). All 73 scatterers that fall within the Australian mainland are located less than 156 km away from such a boundary, and 95% are located within 100 km (Fig. 4c-d). If the same number of scatterers were distributed randomly across the continental mainland, we would typically expect the maximum distance of scatterers to be twice as far away, up to 310 km from the boundary, and the number within 100 km to be 15% less. A two-sample Kolmogorov–Smirnov test [30–32] between the CDF of the locations of the observed scatterers and the mean CDF of 100 random distributions returns a p-value of 0.0006. This suggests that the null hypothesis; that the randomly distributed points and the continental mainland scatterers are from the same continuous distribution, can be rejected at the 0.06% significance level. It can therefore be implied that the spatial correlation is significantly better than random.

Looking more closely at where the continental scatterers are found, several appear to be associated with the Proterozoic orogenic blocks and deformation belts of central and northern Australia (Fig. 3b). These tectonic features are associated with prominent gravity anomalies (Fig. 3c), indicating that they represent major crustal structures with potentially deeper expressions in the mantle lithosphere also [34]. Multiple scatterers can be found on the edge of the strongest gravity anomalies, including the east-west trending Musgrave (Mu) and Arunta (Ar) blocks in central Australia (dashed white circle Fig. 3c), and the north-south trending Darling Fault at the southwest corner of the Yilgarn Craton (YC). Interestingly, there are several large amplitude scatterers associated with the Kimberley (K) region of northwestern Australia, which has been

110 argued to be a small cratonic block underlain by an Archean mantle root [2,35]. Within the
111 submerged continental area of Te Riu-a-Māui/Zealandia a correspondence with topographic
112 variations at the surface can also be seen (Fig. 3a), particularly near New Caledonia (NC) and
113 along the New Caledonia Trough and Norfolk Ridge. This hints at an association with the
114 internal geological architecture of Te Riu-a-Māui/Zealandia similar to that found within
115 Australia.

116 As well as old tectonic boundaries within the continental interior and along its margins,
117 as would be expected multiple scatterers can be found at present day plate boundaries (white
118 dashed lines and white circles; Fig. 3a), such as the New Hebrides Trench (NHT).

119

120 **Discussion**

121 *Errors and uncertainties on the interpretation of Quasi-Love waves*

122 It is important to first consider the uncertainties associated with the analysis of QL waves
123 before making any physical interpretations. A brief summary is provided here in terms of the
124 mechanism, magnitude, depth, and location (for a more detailed description please see Methods).
125 Numerous studies have demonstrated that QL waves are most efficiently generated by lateral
126 gradients in seismic anisotropy (i.e. changes in either the strength or orientation of seismic
127 anisotropy), and are difficult to reproduce with purely isotropic velocity changes [36–39]. Higher
128 mode Rayleigh waves with velocities faster than the fundamental mode may potential interfere
129 within the selected time window, but shallow earthquakes (<50 km) should preferentially excite
130 the fundamental mode rather than higher modes [40]. In addition all QL wave detections are
131 visually inspected to ensure similarity in waveform shape with the Love wave (G1).

The magnitude of the QL wave (i.e. size of the symbols in Fig. 3), is expressed as the relative amplitude between QL and G1. This magnitude is a function of both the strength of the lateral anisotropic gradient and the propagation azimuth relative to the anisotropic geometry. If the propagation direction is parallel or perpendicular to the symmetry axis then the amplitude will be zero. A particularly large QL amplitude is therefore indicative of the presence of a strong gradient but a small amplitude, or even absence of a QL wave entirely, is not conclusive evidence of a weak or non-existent gradient. It is therefore not possible to directly interpret the amplitudes of the observations.

Depth sensitivity kernels calculated for a QL wave with a dominant frequency of 0.01 Hz (100 s) suggest a broad range of sensitivity throughout the upper mantle, with a peak around 100-200 km depth (refer to Fig. S1 of Levin et al. (2007), Fig. 9 of Chen and Park (2013)). While potential contributions from shallower or deeper depths cannot be entirely ruled out, the source of the QL waves most likely resides within the upper mantle, and not within the crust.

The location of the QL scattering source is found by back-projection along the great-circle path (Figs. 1, S2, S5). Potential location errors are estimated to be on the order of 100 km, considering the typical wavelength of 100s surface waves, the results of numerical experiments[18], potential deviations from the great-circle path, and assumptions made the uniformity of the average Rayleigh and Love phase velocities between source and receiver (refer to Methods for details). This is consistent with the spatial distribution of results found relative to certain tectonic and geological features (Figs. 3-4, S9).

New implications for the upper mantle beneath the Australian continent and its margins

The results of this study reveal the widespread presence of lateral anisotropic gradients capable of generating QL waves. The location of such gradients appear closely linked to past tectonic boundaries, both within the continental interior and along the rifted margins. Such features visible from the Earth's surface, by inference, must also extend to depth within the upper mantle. Considering the peak sensitivity of Love-to-Rayleigh scattering at 100s period is expected to be between 100-200 km depth [18,22], this depth range would sample the old thick cratonic lithosphere in central and western Australia (light colors; Fig. 3d), while for eastern Australia the lithosphere is younger (Phanerozoic) and much thinner, ~75km [41]. Except in regions of thick continental lithosphere, the QL scatterers should therefore correspond to lateral anisotropic gradients in the asthenosphere, where olivine LPO is expected to develop through mantle flow [42].

A large number of scatterers in this dataset are associated with continental margins (Figs. 3a-b, 4a-b), similar to the findings of Servali et al., (2020) who detected pervasive scatterers along the eastern North America passive margin. For western and southern Australia the margin is co-located with the edge of the thick continental lithosphere (Fig. 3d, Fig. 5). QL scatterers along this boundary may therefore simply reflect the transition from active flow in the asthenosphere to anisotropy fossilized within the lithosphere, which is supported by the first-order patterns seen in tomographic models of azimuthal anisotropy (Figs. 3d, S11). Alternatively a significant step in lithospheric thickness may trigger edge-driven convection (EDC) at the margin [43], which can generate high-strain rates and localize dislocation-creep deformation capable of overprinting LPO anisotropy to beneath the lithospheric step [44]. For the southern Australian margin, geodynamical models have suggested the formation of broad upwellings in the region behind the trailing edge of the continent due to EDC [45], which may potentially explain

177 the broad zone of QL scatterers in this region. Numerous scatterers along the eastern margin of
178 Australia, and the western margin of Te Riu-a-Māui/Zealandia, are however less easy to explain
179 given that the lithosphere appears consistently thin (<100 km) across this region. This may
180 instead hint at a fundamental difference between how continental versus oceanic lithosphere
181 couples to the underlying asthenosphere, perhaps in terms of differences in viscosity [46].
182 Alternatively finer-scale variations in lithospheric thickness along the margins may exist than
183 those currently resolved in Figure 3d. Such small-scale 3D topography on the lithosphere-
184 asthenosphere boundary may locally divert or disrupt the mantle flow-field, such as localized
185 EDC processes proposed at the Newer Volcanics Province in SE Australia [44,47]. Recent modeling
186 work [48] suggests that even when the edge of the continent is parallel with the background mantle
187 flow field (as is generally thought to be the case for eastern Australia) dynamical instabilities in
188 mantle flow can still be found at the edges of thick continental lithosphere, and may be enhanced
189 where there are smaller-scale variations in the geometry of the boundary. It remains to be seen
190 however whether the same effect could be generated beneath eastern Australia with only small
191 changes in lithospheric thickness and/or viscosity.

192 Another significant finding of this study is the presence of numerous QL scatterers
193 associated with the major geological provinces of Australia (Fig. 3). Many of these scatterers are
194 located within thick cratonic lithosphere (Fig. 3d), and are associated with Archean-Proterozoic
195 terranes and past orogenies (Fig. 3b). This suggests QL scatterers are sensitive to lithospheric
196 anisotropy frozen-in since the last deformational episode, and therefore that they reflect the
197 evolution of the continent. Furthermore this implies that geological boundaries are preserved
198 over billions of years not only in the crust but also at deeper depths as anisotropic gradients in
199 the lithospheric mantle. If fossilized lithospheric anisotropy is pervasive, yet heterogenous with

strong lateral gradients, including the potential for multiple layers to exist within cratonic lithosphere[49], this would add interference to the SKS splitting accrued from the strong active flow in the underlying mantle, causing a loss of coherency in the overall signal. This may explain the long-standing conundrum as to why SKS splitting is perplexingly weak and complex across Australia [9–11], despite fast Australian plate motion, and strong azimuthal anisotropy imaged beneath the continent (Figs. 3d, S11) [7,8,12]. Further studies to constrain lithospheric anisotropy may therefore help to decode the complex SKS splitting, as well as provide further insights on the past deformational history of continent.

Conclusion

Observations of QL waves have revealed extensive lateral anisotropic gradients beneath the Australian continent and its margins that have otherwise, until now, been impossible to resolve with smooth seismic tomographic methods (e.g. Fig. 3d). Based on the newly acquired results, it is speculated that at the continental margins small-scale convective processes, such as EDC, or localized disruptions to the mantle flow field, may be occurring where the lithosphere transitions from continental to oceanic. Alternatively QL scattering may be explained by the difference between fossil anisotropy in old thick continental lithosphere and active flow in the oceanic asthenosphere. However, this is harder to justify where the continental lithosphere is younger and thinner on either side of the Tasman Sea. In the future QL scatterers may be used as a predictive tool, helping to constrain the geophysical signature of major crustal/lithospheric structures at depth, such as those currently hidden under cover [50], and in particular in identifying those with deep mantle connections that may suggest potential for mineralization [31,51].

Methods

Overview of data selection and processing

Earthquakes from 1994-2020 of magnitude >6.5, depth <50 km, and in the epicentral distance range of 70°-180° were selected to ensure large amplitude surface waves and enough separation to distinguish QL from R1. All data were low-pass filtered at 100s (0.01Hz) to amplify the fundamental Love and Rayleigh wave components and suppress overtones. Following previous studies, the delay time (δt) between the QL and G1 is calculated using the cross-correlation technique [18,20,27]. In the final step the delay time is converted to distance (see Fig. 1b), and back-projected along the great-circle path to determine the location of the scatterer. If the polarization of the surface waves suggests a deviation from the great-circle path of more than 10° then the result is discarded (Fig. S8). In this study a few modifications have been made to the cross-correlation technique to improve detection and measurement quality. These are outlined in further detail below along with a more detailed description of the methodology.

Strategy for Detection and Measurement of Quasi-Love Waves

Data for each event is requested from the IRIS Data Management Centre (ds.iris.edu/) for 5000 seconds following the origin time. After low-pass filtering at 0.01Hz, seismograms are rotated into the vertical, radial, and transverse, and normalized by the maximum amplitude on each component. The maximum on the transverse signifies the fundamental Love wave (G1), and on the vertical the fundamental Rayleigh wave (R1), indicated by the vertical dashed green and dashed blue lines in Fig. S1. Initial quality control restricts events to those with a signal-to-noise ratio (SNR) of the Love wave greater than 5, where the 'noise' amplitude is determined by the first 300 seconds of the seismogram. A cut-off of 5 was determined empirically from the

data. In general large amplitude Love waves are a necessary pre-requirement to generating observable QL waves, and thus detections are more likely in the Love radiation maxima (and Rayleigh radiation minima).

Most previous studies only measure QL waves on the vertical component even though the particle motion is elliptical and distributed across both the vertical and radial components (Fig. S1b-c). Same as for R1, for QL, the vertical and radial components are 90° out of phase. The first derivative of the radial component (dashed red line Fig. S1d) matches the vertical component. This is a useful diagnostic feature. Any seismograms that do not display this characteristic during the visual inspection process are discarded, and the QL wave must be clearly visible on both components, not just the vertical. Furthermore, stacking of the vertical component with the derivative of the radial component amplifies the QL (and R1) while dampening the noise (magenta line Fig. S1e). This improves both the visibility and confidence of the QL detection.

The next step is to cross-correlate this QL stack with G1 on the transverse component. Fig. S1f shows the absolute amplitude of the cross-correlation (thin black line) as a function of lag time relative to the position of G1. Peaks of this cross-correlation function (i.e. maxima, where the derivative equals zero) are identified by blue crosses and connected by a new blue curve. Peaks in this new curve are then selected and highlighted by blue circles. Typically the largest peak is associated with the correlation between G1 and R1 (as seen in Fig. S1f). The QL peak, if present, is a secondary peak located before the highest R1 peak but after the G1 arrival (indicated by dashed green line). The inferred QL delay time is marked by a green asterisk and dotted green line. The time shifted Love wave is plotted for comparison with the QL stack in Fig. S1e.

All seismograms and cross-correlation functions are visually inspected for quality based on the criteria outlined above. Only those with a clearly visible and distinct QL wave are kept. It is possible however that multiple QL waveforms may appear in one seismogram if multiple scatterers are located along the great circle path. In such cases, for simplicity, the first QL wave, closest to G1, and therefore closest to Australia is recorded.

The last step in the process is to convert the delay time (δt) into distance and back-project the location of the scatterer along the great-circle path. Considering that the QL wave travels distance, δx, of the total path, Δ, (Fig. 1a) with the slower Rayleigh wave phase velocity (V_R), the delay time can be expressed as:

$$\delta t = \frac{\delta x}{V_R} - \frac{\delta x}{V_L} \quad (1)$$

where V_L is the Love wave phase velocity. To negate having to use either an average guess for the phase velocities or calculate individually for every seismogram, the following substitution can be made,

$$\delta t = \frac{\delta x (t_R - t_L)}{\Delta} \quad (2)$$

where Δ is the epicentral distance between source and receiver, and $t_R - t_L$ is the time delay between the Rayleigh (R1) and Love (G1) waves. Simply rearranging this equation for δx gives,

$$\delta x = \frac{\delta t \, \Delta}{(t_R - t_L)} \quad (3)$$

The scatterer distance is therefore independent of the absolute phase velocities or the arrival times, and only depends on the relative time difference between G1 and R1. This is useful given the exact start of the R1 is difficult to determine, especially considering likely overlap with QL. Instead the time difference between the maximum amplitude of G1 and R1 can be utilized, which is much easier to calculate from the seismogram.

Errors and uncertainties on the interpretation of Quasi-Love waves

In this study the term 'Quasi-Love waves' refers to surface wave polarization anomalies that are characteristic of Love-to-Rayleigh scattering. This is distinct from distortions or rotations of the polarization of surface waves by azimuthal anisotropy that are sometimes also called 'quasi-Love' waves or 'quasi-Rayleigh' waves elsewhere in the literature [14–16]. Such polarization distortions are analogous to the terminology of 'quasi-P' and 'quasi-S' when body-wave polarizations are altered by Earth 3D heterogeneity [17]. In such polarization-distortion cases, the 'quasi-Love' wave will exhibit particle motion that is still mostly transverse polarized but with a small added vertical component (see Figure 2 of [16]). In contrast, Love-to-Rayleigh scattering generates Quasi-Love waves that are predominantly polarized in the vertical-radial plane, displaying ellipticity characteristic of Rayleigh waves with a 90° phase lag between the vertical and radial components [17]. By comparing the waveform shape of the QL wave on both the vertical component and the first-derivative of the radial component during the measurement process (e.g. Fig. S1d) ensures the presence of characteristic Rayleigh wave motion as expected for QL wave scattering. Incorrect interpretations due to slight polarization-distortions are thus considered unlikely in the present dataset.

Previous studies have shown that Love-to-Rayleigh scattering is most efficiently generated by lateral gradients in seismic anisotropy (i.e. changes in seismic anisotropy either in strength or orientation) rather than changes in isotropic structure [36–39]. Lateral anisotropic gradients of only 3-5% are enough to generate QL waves with 5-10% amplitude of the fundamental Love wave [19,38], compared to unrealistic perturbations of 20% or more which would be required to produce the same effect with isotropic velocity changes only [36,37]. Additionally QL waves are not typically seen in synthetic seismograms generated from velocity models without

lateral variations in azimuthal anisotropy (Fig. S6) [20,26,27]. It is worth noting that lateral anisotropic gradients will also cause Rayleigh-to-Love scattering, generating Quasi-Rayleigh waves, in addition to Quasi-Love waves [17,52]. Such Quasi-Rayleigh waves will appear on the transverse component trailing G1 and thus are more challenging and less commonly studied compared to QL waves that arrive ahead of R1 on the vertical and radial components [52]. As a relatively large amplitude of G1 is a pre-requirement of this study (SNR>5), the amplitude of R1 is often comparatively less, and thus Quasi-Rayleigh waves are not expected to be visible on the same seismograms as prominent QL waves (Fig. S1).

The relative amplitude between the QL wave and the fundamental Love wave is represented via the cross-correlation amplitude, which is used to determine the symbol size in Fig. 3. QL amplitude is dependent not only on the strength of the anisotropic gradient but also on the anisotropic geometry relative to the propagation path. Maximum QL conversion will occur when the propagation azimuth is 45° to the symmetry axis, and zero conversion when the propagation azimuth is either parallel or perpendicular [20,53]. This creates a symmetric four-lobed radiation pattern with both positive and negative polarities of the QL wave, which in theory could be used to infer not only the location of an anisotropic gradient but also the geometry of anisotropy. It is safe to say that large QL amplitudes can be interpreted as the existence of a strong gradient in anisotropy but smaller amplitudes do not necessarily equate to a weaker gradient. Likewise a lack of detection of QL waves is not conclusive evidence that anisotropic gradients do not exist along the great circle path. The angle between the propagation path and the geometry of the anisotropy may simply be non-optimal for Love-to-Rayleigh scattering to occur.

While lateral variations in seismic anisotropy are the most likely cause of the QL wave scatterers, an important consideration is at what depth they are generated. Depth sensitivity

kernels calculated for QL wave scattering with a dominant frequency of 0.01 Hz (100 s) suggest a broad range of sensitivity throughout the upper mantle but with a peak around 100-200 km depth (refer to Fig. S1 of Levin et al. (2007), Fig. 9 of Chen and Park (2013)). While potential contributions from shallower or deeper depths cannot be entirely ruled out, the source of the QL waves most likely resides within the upper mantle, and not within the crust.

As well as the depth, there is also a degree of uncertainty associated with the horizontal location of the QL wave source. Firstly, the width of the lateral anisotropic gradient cannot be exactly determined. For example, a wide gradational zone can produce the same signal as a sharp localized gradient, but both are represented as a point scatterer at the center of the lateral gradient distribution [20]. Secondly, the smallest feature that can be resolved is likely on the order of 1/4th of the wavelength [18]. Surface waves with a period of 100s have a wavelength of ~400 km, suggesting ~100 km resolution. This is consistent with numerical experiments based on simple anisotropic models with an equatorial band of 4% azimuthal anisotropy, in which the source of the QL scatterer could be correctly located to within 100 km following a similar methodology to that applied here[18].

The real Earth however is much more complex than such idealized models and location errors may be influenced by 3D heterogeneity. In particular 3D velocity structure may cause deviations from the great circle path (e.g. multi-pathing), which could result in a location error when the QL wave source is back-projected. In order to limit this, a comparison is made between the polarization of the surface waves and the source-receiver back-azimuth. Any events with deviations greater than 10° are thrown out from the dataset, but most are in agreement to within a few degrees (Fig. S8). Slight rotations away from the radial/vertical (Rayleigh) and transverse (Love) polarizations are to be expected when in the presence of seismic anisotropy [14–17].

Nonetheless, a maximum deviation of 10° from the great circle path would result in a location error of 390 km for a QL wave scatterer at a typical distance of 20° from the receiver (Fig. S8). A typical deviation of 2° would however cause a location error of <100 km.

A location error may also result regarding the assumption that the average Rayleigh and Love phase velocities between the QL scatterer and the seismic station are the same as the average phase velocities along the entire great-circle path. Considering that many of the propagation paths cross an ocean basin before generating a QL wave and then continue through mainly continental regions after scattering at the ocean-continent boundary, this may cause the phase velocities along the respective path segments to substantially differ, either due to changes in isotropic or anisotropic properties or both. If the average phase velocities were 5% higher between the QL scatter and the receiver (i.e. δx), than between the earthquake source and the receiver (i.e. Δ), then this would directly correspond to a 5% error in the scatterer location as a function of distance along the great circle path. For example, if a typical QL scatterer is estimated to be 20° away from the receiver, then a 5% velocity error would equate to a distance error of 1° (~110 km).

Overall based on the above considerations, typical location errors are expected to be on the order of 100 km but the further away the QL scatterers are the size of the error likely increases. This may be supported by the data as Fig. 4 suggests that QL scatterers are preferentially located near the ocean-continent boundary to within 400-500 km, and with geological provinces to within 100-150km, based upon the steepness of the CDF curve relative to the random distributions.

Of further note, the methodology applied here is based upon detecting a single scatterer located closer to the receiver than to the source. This ensures enough separation from the

Rayleigh wave on the radial and vertical components in order to be able to identify the QL wave. If a QL scatterer is located near the source then the QL arrival will overlap with the Rayleigh wave making it hard to distinguish. Likewise, in the cases where more than one potential QL wave is identifiable on the seismogram, potentially due to multiple lateral gradients in seismic anisotropy along the propagation path, only that which is closest to the receiver is included in the dataset as it is the easiest to distinguish. If the seismogram contains multiple closely arriving QL waves generating a complex overlapping signal, then this will be discarded during the quality control process as the QL wave is required to have a similar waveform shape as G1 (Fig. S1).

Lastly, it is possible for QL waves to resemble higher-mode Rayleigh waves [26,54]. In this study only shallow events less than 50 km depth are considered are these should primarily excite the fundamental modes rather than overtones, and all seismograms are low pass filtered at 100s which should aid separation of the modes [55]. During the quality control process, the requirement that the QL wave should have a similar waveform shape to G1 (see Fig. S1), should also help distinguish potential interference from higher mode Rayleigh waves, as these would not be expected to possess the same waveform shape as G1. Following these conditions, synthetic seismograms demonstrate that the observed QL waves are unlikely to be the result of higher mode Rayleigh waves (Fig. S6) [18,26,27].

Data Availability

The seismic data used in this study is from the Australian National Seismograph Network (network code AU; www.fdsn.org/networks/detail/AU/), and can be freely obtained via the Data Management Center of Incorporated Research Institutions for Seismology (ds.iris.edu/). A full list of results is provided in Supplementary Table S1.

Acknowledgements

Figures were made using Generic Mapping Tools [56], GeoMapApp (www.geomapapp.org), and AUSGIN (portal.geoscience.gov.au). This work was supported by grant DE190100062 from the Australian Research Council. The manuscript benefitted from constructive comments from Nicolas Flament and two anonymous reviewers, as well as helpful conversations with Ana Ferreira, Mark Hoggard, Rhodri Davies, Malcolm Sambridge, and Brian Kennett.

Author Contributions and Competing Interests Declaration

The sole author of this work, C.M. Eakin, conducted the study in its entirety. The author declares no competing interests.

References

1. Myers, J. S., Shaw, R. D. & Tyler, I. M. Tectonic evolution of Proterozoic Australia. *TECTONICS* **15**, 1431–1446 (1996).
2. Betts, P. G., Giles, D., Lister, G. S. & Frick, L. R. Evolution of the Australian lithosphere. *Aust. J. Earth Sci.* **49**, 661–695 (2002).
3. Kennett, B. L. N. & Blewett, R. S. Lithospheric framework of Australia. *Episodes* **35**, 9–12 (2012).
4. Seton, M. *et al.* Global continental and ocean basin reconstructions since 200Ma. *Earth-Science Reviews* **113**, 212–270 (2012).
5. Falvey, D. A. & Mutter, J. C. Regional plate tectonics and the evolution of Australia's passive continental margins. *BMR J. Aust. Geol. Geophys.* **6**, 1–29 (1981).

6. Sandiford, M. & Quigley, M. TOPO-OZ: Insights into the various modes of intraplate deformation in the Australian continent. *Tectonophysics* **474**, 405–416 (2009).

7. Debayle, E., Kennett, B. & Priestley, K. Global azimuthal seismic anisotropy and the unique plate-motion deformation of Australia. *Nature* **433**, 509–512 (2005).

8. Debayle, E., Dubuffet, F. & Durand, S. An automatically updated S -wave model of the upper mantle and the depth extent of azimuthal anisotropy. *Geophys. Res. Lett.* **43**, 674–682 (2016).

9. Heintz, M. & Kennett, B. L. N. Continental scale shear wave splitting analysis: Investigation of seismic anisotropy underneath the Australian continent. *Earth Planet. Sci. Lett.* **236**, 106–119 (2005).

10. Heintz, M. & Kennett, B. L. N. The apparently isotropic Australian upper mantle. *Geophys. Res. Lett.* **33**, L15319 (2006).

11. Bello, M., Cornwell, D. G., Rawlinson, N. & Reading, A. M. Insights into the structure and dynamics of the upper mantle beneath Bass Strait, southeast Australia, using shear wave splitting. *Phys. Earth Planet. Inter.* **289**, 45–62 (2019).

12. Yoshizawa, K. & Kennett, B. L. N. The lithosphere-asthenosphere transition and radial anisotropy beneath the Australian continent. *Geophys. Res. Lett.* **42**, 3839–3846 (2015).

13. Park, J. & Yu, Y. Seismic Determination of Elastic Anisotropy and Mantle Flow. *Science.* **261**, 1159–1162 (1993).

14. Crampin, S. Distinctive Particle Motion of Surface Waves as a Diagnostic of Anisotropic Layering. *Geophys. J. Int.* **40**, 177–186 (1975).

15. Maupin, V. Surface waves in weakly anisotropic structures: on the use of ordinary or quasi-degenerate perturbation methods. *Geophys. J. Int.* **98**, 553–563 (1989).

16. Tanimoto, T. The azimuthal dependence of surface wave polarization in a slightly anisotropic medium. *Geophys. J. Int.* **156**, 73–78 (2004).

17. Maupin, V. & Park, J. Theory and observations—Seismic anisotropy. in *Treatise on Geophysics* (ed. Schubert, G.) 277–305 (Elsevier, 2015). doi:10.1016/B978-0-444-53802-4.00007-5

18. Chen, X. & Park, J. Anisotropy gradients from QL surface waves: Evidence for vertically coherent deformation in the Tibet region. *Tectonophysics* **608**, 346–355 (2013).

19. Yu, Y., Park, J. & Wu, F. Mantle anisotropy beneath the Tibetan Plateau: evidence from long-period surface waves. *Phys. Earth Planet. Inter.* **87**, 231–246 (1995).

20. Rieger, D. M. & Park, J. USArray observations of quasi-Love surface wave scattering: Orienting anisotropy in the Cascadia plate boundary. *J. Geophys. Res.* **115**, B05306 (2010).

21. Kobayashi, R. & Nakanishi, I. Location of Love-to-Rayleigh conversion due to lateral heterogeneity or azimuthal anisotropy in the upper mantle. *Geophys. Res. Lett.* **25**, 1067–1070 (1998).

22. Levin, V., Park, J., Lucente, F. P., Margheriti, L. & Pondrelli, S. End of subduction in northern Apennines confirmed by observations of quasi-Love waves from the great 2004 Sumatra-Andaman earthquake. *Geophys. Res. Lett.* **34**, 1–5 (2007).

23. Margheriti, L. *et al.* Large-scale coherent anisotropy of upper mantle beneath the Italian peninsula comparing quasi-Love waves and SKS splitting. *J. Geodyn.* **82**, 26–38 (2014).

24. Levin, V. & Park, J. Quasi-Love phases between Tonga and Hawaii: Observations, simulations, and explanations. *J. Geophys. Res. Solid Earth* **103**, 24321–24331 (1998).

25. Yu, Y. & Park, J. Hunting for azimuthal anisotropy beneath the Pacific Ocean region. *J.*

Geophys. Res. **99**, 15399 (1994).

26. Cheng, W., Hu, X. G. & Liu, L. T. Anisotropy Gradients in the Middle of the Ross Sea Embayment, West Antarctica: Evidence From QL Scattered Surface Waves. *Geophys. Res. Lett.* **48**, e2020GL091232 (2021).

27. Servali, A., Long, M. D., Park, J., Benoit, M. H. & Aragon, J. C. Love-to-Rayleigh scattering across the eastern North American passive margin. *Tectonophysics* **776**, 228321 (2020).

28. Müller, R., Sdrolias, M., Gaina, C. & Roest, W. Age, spreading rates, and spreading asymmetry of the world's ocean crust. *Geochemistry, Geophys. Geosystems* **9**, 18–36 (2008).

29. Gaina, C., Müller, R. D., Brown, B. & Ishihara, T. Micro-continent formation around Australia. in *The Evolution and Dynamics of the Australian Plate* (eds. Hillis, R. & Müller, R. D.) 405–416 (Geological Society of Australia, 2003).

30. Kolmogorov, A. Sulla determinazione empirica di una legge di distribuzione. *G. della Ist. Ital. degli Attuari* **4**, 83–91 (1933).

31. Hoggard, M. J. *et al.* Global distribution of sediment-hosted metals controlled by craton edge stability. *Nat. Geosci.* **13**, 504–510 (2020).

32. Davies, D. R., Goes, S. & Sambridge, M. On the relationship between volcanic hotspot locations, the reconstructed eruption sites of large igneous provinces and deep mantle seismic structure. *Earth Planet. Sci. Lett.* **411**, 121–130 (2015).

33. Raymond, O. L., Totterdell, J. M., Woods, M. A. & Stewart, A. J. Australian Geological Provinces 2018.01 edition. (2018). doi:http://pid.geoscience.gov.au/dataset/ga/116823

34. Kennett, B. L. N. & Iaffaldano, G. Role of lithosphere in intra-continental deformation:

Central Australia. *Gondwana Res.* **24**, 958–968 (2013).

35. Graham, S., Lambert, D., Shee, S., Smith, C. & Reeves, S. Re-Os isotopic evidence for Archean lithospheric mantle beneath the Kimberley block, Western Australia. *Geology* **27**, 431–434 (1999).

36. Kobayashi, R. Polarization anomaly of Love waves caused by lateral heterogeneity. *Geophys. J. Int.* **135**, 893–897 (1998).

37. Park, J. & Yu, Y. Anisotropy and coupled free oscillations: simplified models and surface wave observations. *Geophys. J. Int.* **110**, 401–420 (1992).

38. Yu, Y. & Park, J. Upper mantle anisotropy and coupled-mode long-period surface waves. *Geophys. J. Int.* **114**, 473–489 (1993).

39. Oda, H. & Onishi, S. The effect of regional variation of lattice preferred orientation on surface waveforms. *Geophys. J. Int.* **144**, 247–258 (2001).

40. Ekström, G. A global model of Love and Rayleigh surface wave dispersion and anisotropy, 25-250s. *Geophys. J. Int.* **187**, 1668–1686 (2011).

41. Kennett, B. L. N. & Salmon, M. AuSREM: Australian Seismological Reference Model. *Aust. J. Earth Sci.* **59**, 1091–1103 (2012).

42. Nicolas, A. & Christensen, N. I. Formation of anisotropy in upper mantle peridotites: A review. in *Composition, structure and dynamics of the lithosphere-asthenosphere system* (eds. Fuchs, K. & Froidevaux, C.) 111–123 (American Geophysical Union, 1987). doi:10.1029/GD016p0111

43. King, S. D. & Anderson, D. L. Edge-driven convection. *Earth Planet. Sci. Lett.* **160**, 289–296 (1998).

44. Davies, D. R. & Rawlinson, N. On the origin of recent intraplate volcanism in Australia.

Geology **42**, 1031–1034 (2014).

45. Farrington, R. J., Stegman, D. R., Moresi, L. N., Sandiford, M. & May, D. A. Interactions of 3D mantle flow and continental lithosphere near passive margins. *Tectonophysics* **483**, 20–28 (2010).

46. Conrad, C. P., Behn, M. D. & Silver, P. G. Global mantle flow and the development of seismic anisotropy: Differences between the oceanic and continental upper mantle. *J. Geophys. Res.* **112**, B07317 (2007).

47. Rawlinson, N., Davies, D. R. & Pilia, S. The mechanisms underpinning Cenozoic intraplate volcanism in eastern Australia: Insights from seismic tomography and geodynamic modeling. *Geophys. Res. Lett.* **44**, 9681–9690 (2017).

48. Duvernay, T., Davies, D. R., Mathews, C., Gibson, A. H. & Kramer, S. C. Linking Lithospheric Structure, Mantle Flow and Intra-Plate Volcanism. *Earth Sp. Sci. Open Arch.* (2021). doi:10.1002/ESSOAR.10504315.1

49. Yuan, H. & Romanowicz, B. Lithospheric layering in the North American craton. *Nature* **466**, 1063–1068 (2010).

50. Korsch, R. J. & Doublier, M. P. Major crustal boundaries of Australia. (2015). doi:10.4225/25/555C181CC0EAE

51. Hronsky, J. M. A., Groves, D. I., Loucks, R. R. & Begg, G. C. A unified model for gold mineralisation in accretionary orogens and implications for regional-scale exploration targeting methods. *Miner. Depos.* **47**, 339–358 (2012).

52. Pettersen, Ø. & Maupin, V. Lithospheric anisotropy on the Kerguelen hotspot track inferred from Rayleigh wave polarisation anomalies. *Geophys. J. Int.* **149**, 225–246 (2002).

53. Park, J. Free oscillations in an anisotropic earth: path-integral asymptotics. *Geophys. J. Int.* **129**, 399–411 (1997).

54. Kobayashi, R. Polarization anomalies of Love waves observed in and around Japan. *Earth, Planets Sp.* **54**, 357–365 (2002).

55. Hariharan, A., Dalton, C. A., Ma, Z. & Ekström, G. Evidence of Overtone Interference in Fundamental-Mode Rayleigh Wave Phase and Amplitude Measurements. *J. Geophys. Res. Solid Earth* **125**, e2019JB018540 (2020).

56. Wessel, P., Smith, W. H. F., Scharroo, R., Luis, J. & Wobbe, F. Generic Mapping Tools: Improved Version Released. *Eos, Trans. Am. Geophys. Union* **94**, 409–410 (2013).

57. Bird, P. An updated digital model of plate boundaries. *Geochemistry, Geophys. Geosystems* **4**, 1027 (2003).

58. Amante, C. & Eakins, B. W. ETOPO1 1 arc-minute global relief model: procedures, data sources and analysis. *NOAA Tech. Memo. NESDIS NGDC-24* 19 (2009).

59. Cawood, P. A. & Korsch, R. J. Assembling Australia: Proterozoic building of a continent. *Precambrian Res.* **166**, 1–35 (2008).

60. Sandwell, D. T., Müller, R. D., Smith, W. H. F., Garcia, E. & Francis, R. New global marine gravity model from CryoSat-2 and Jason-1 reveals buried tectonic structure. *Science.* **346**, 65–67 (2014).

Figures

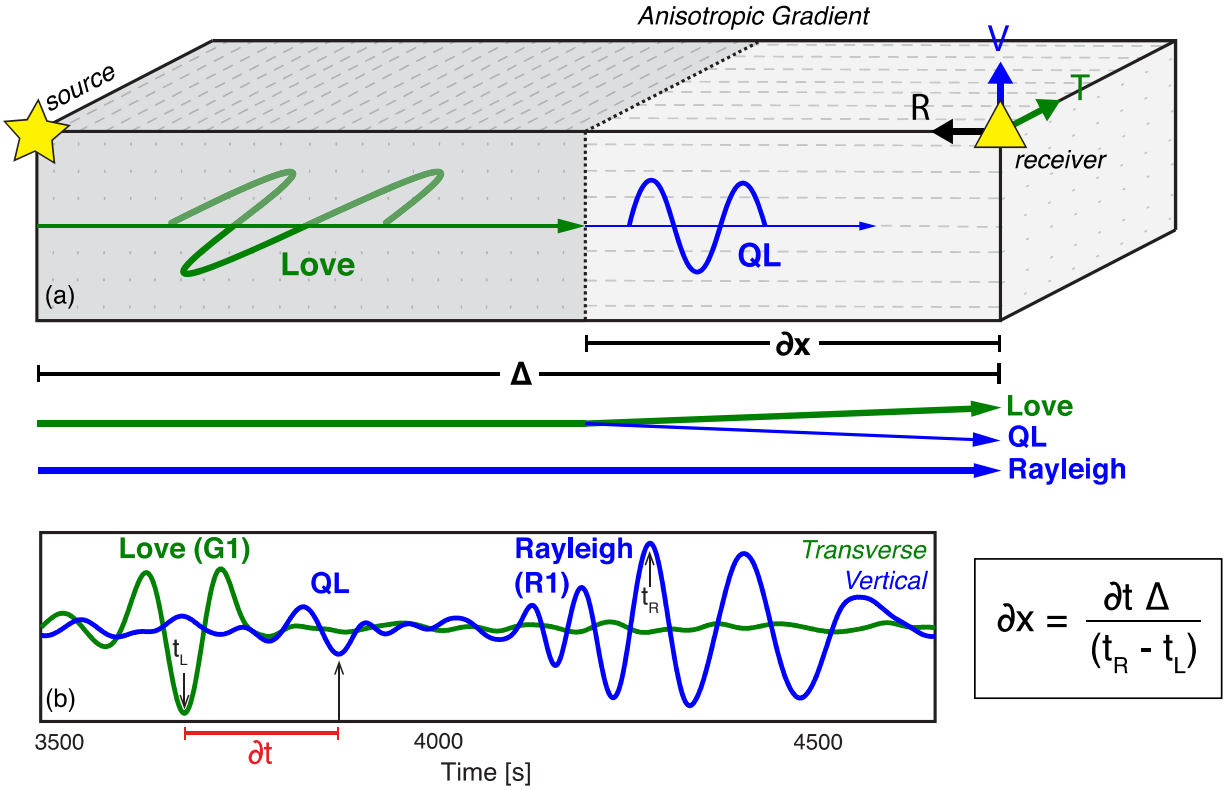

Figure 1. Process of QL wave scattering due to an anisotropic gradient. (a): Schematic illustration of a Love wave with transverse (T) particle motion (indicated in green), which upon encountering a lateral gradient in seismic anisotropy, partially converts into a QL wave with the same phase velocity and vertical (V) particle motion (indicated by blue) as a Rayleigh wave. The fundamental Love (G1) and Rayleigh (R1) waves travel a distance Δ between the source and receiver, whereas the QL wave only travels a distance δx between the scattering location and the receiver. The scattering is caused by a change in strength and/or orientation of the mantle anisotropy, indicated by the grey fabric pattern. (b): Example recording of a QL wave arrival that is found on the vertical component between G1 and R1. The distance to the scattering point (δx) is related to the time delay (δt) between the QL and G1 via the equation shown.

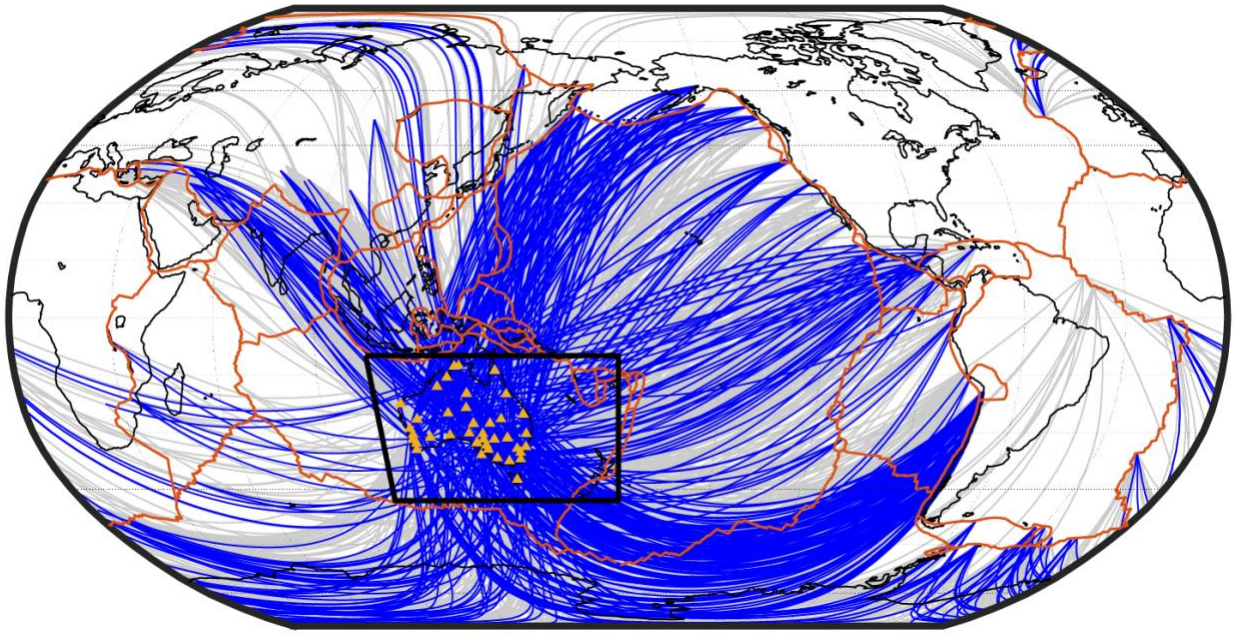

Figure 2. Global distribution of source-receiver paths analyzed for QL waves. Great-circle paths on which QL waves were present are shown in blue, the remainder in grey. The location of anisotropic gradients within the area of interest (black box, Fig. 3) is investigated using 43 seismic receivers (yellow triangles) based within Australia. Plate boundaries (in orange) from [57].

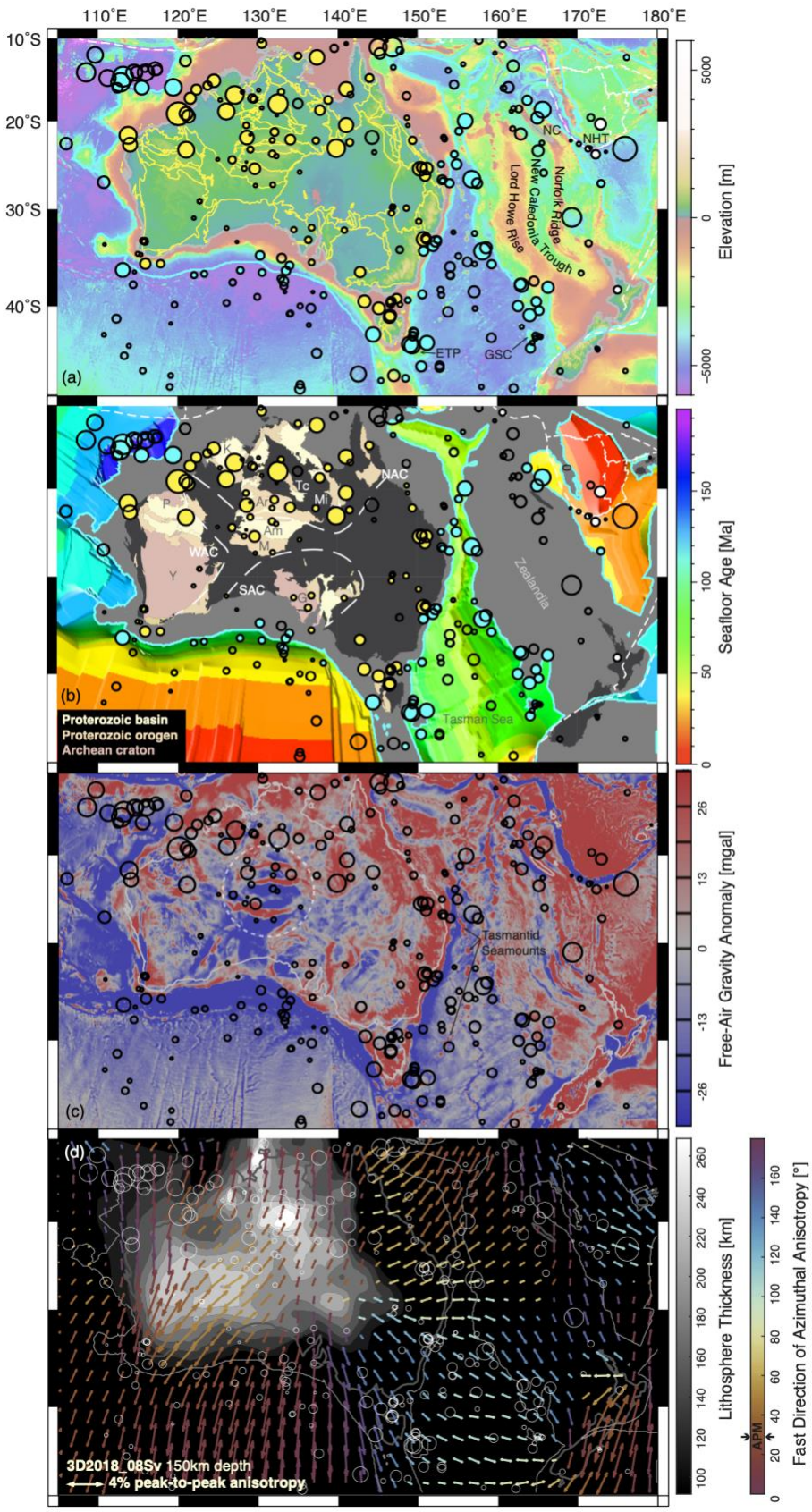
110°E
120°E
130°E
140°E
150°E
160°E
170°E
180°E
10°S
20°S
30°S
40°S
(a)
NC
NHT
New Caledonia Trough
Norfolk Ridge
Lord Howe Rise
ETP
GSC
Elevation [m]
5000
0
−5000
(b)
NAC
Tc
Mi
Ar
Am
WAC
SAC
Zealandia
Tasman Sea
Proterozoic basin
Proterozoic orogen
Archean craton
Seafloor Age [Ma]
150
100
50
0
(c)
Tasmantid Seamounts
Free-Air Gravity Anomaly [mgal]
26
13
0
-13
-26
(d)
3D2018_08Sv 150km depth
4% peak-to-peak anisotropy
Lithosphere Thickness [km]
260
240
220
200
180
160
140
120
100
APM
Fast Direction of Azimuthal Anisotropy [°]
160
140
120
100
80
60
40
20
0

584

Figure 3. QL wave scattering points (black circles) compared to (a): surface topography [58], (b): seafloor age [28], the ocean-continent boundary, and the Precambrian tectonic elements of Australia [59], (c): free-air gravity [60], and (d): azimuthal anisotropy from 3D2018_08Sv [8] and the lithospheric thickness from AuSREM [31,41]. Circles are scaled in size relative to the amplitude of the QL wave. Those which coincide (within a typical error of 100 km) with either a plate boundary (dashed white lines), the ocean-continent margin (solid cyan lines), or geological provinces within Australia (yellow lines) [33], are highlighted by a solid circle with the respective color in (a) and (b). In (a) abbreviations are as follows: ETP- East Tasman Plateau, GSC- Gilbert Seamount Complex, NC- New Caledonia, NHT- New Hebrides Trench. In (b) abbreviations refer to major Precambrian provinces: Am- Amadeus, Ar- Arunta, G- Gawler, K- Kimberley, M- Musgrave, Mi- Mount Isa, P- Pilbara, Tc- Tennant Creek, Y- Yilgarn. White dashed lines show the approximate extent of the West Australian Craton (WAC), North Australian Craton (NAC), and South Australian Craton (SAC). In (c) the large dashed white circle over central Australia highlights the location of prominent E-W trending gravity anomalies. In (d) azimuthal anisotropy is illustrated by the arrows, with colors indicating the fast direction orientation, and the length of the arrow relative to the strength of anisotropy (refer to legend for scale).

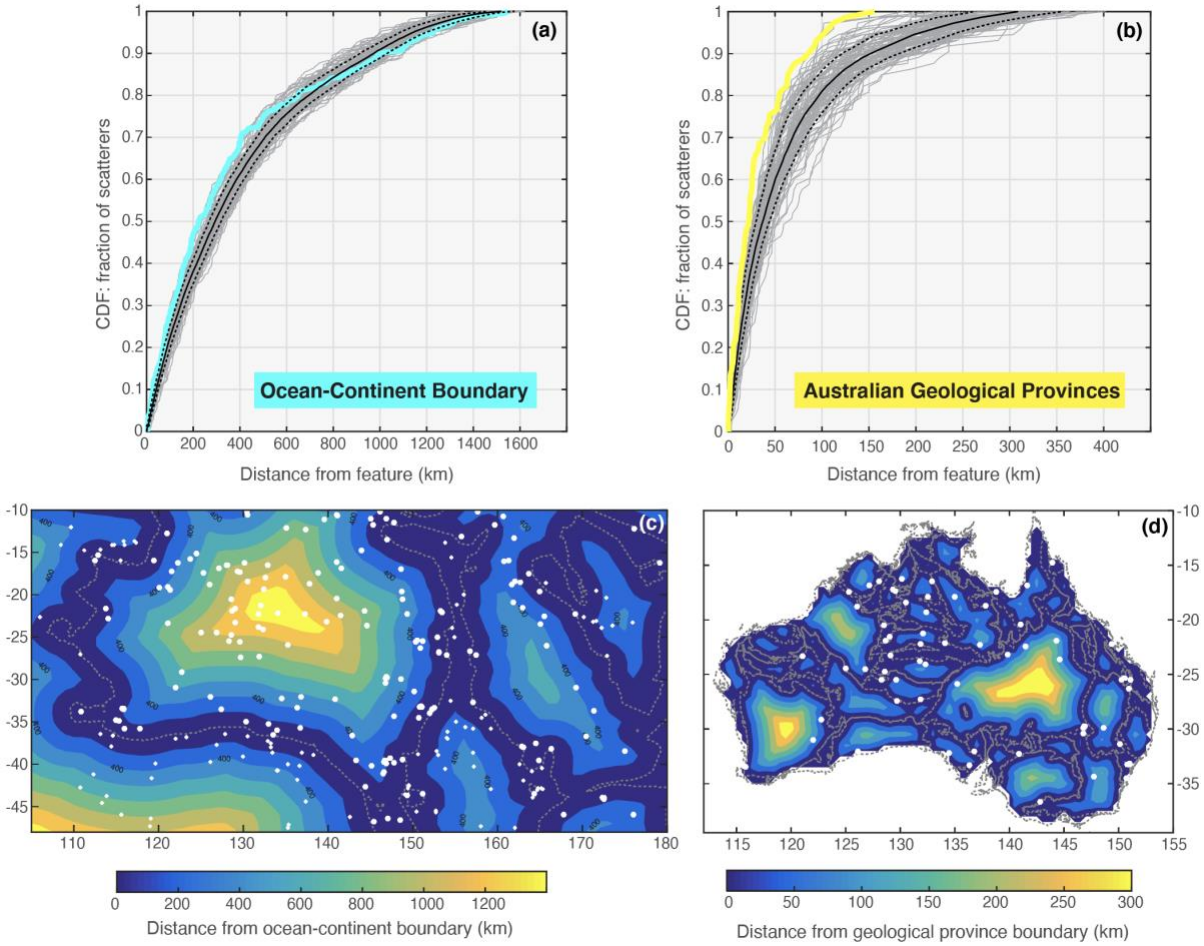

Figure 4. Distance of QL scatterers relative to associated features. (a-b): Cumulative distribution functions (CDF) showing the fraction of all observed QL scatters as a function of distance from the ocean-continent boundary [28] (cyan line) and major geological provinces (yellow line) [33]. The same CDFs are generated for 100 sets of the equivalent number of points randomly located across the study area (thin grey lines), alongside their mean (solid black line) and one standard deviation (dotted black line). (c-d) Maps showing spatial distribution of QL scatterers (small white symbols) compared to contours of the distance from either the ocean-continent boundary (c) or the geological province boundaries (d).

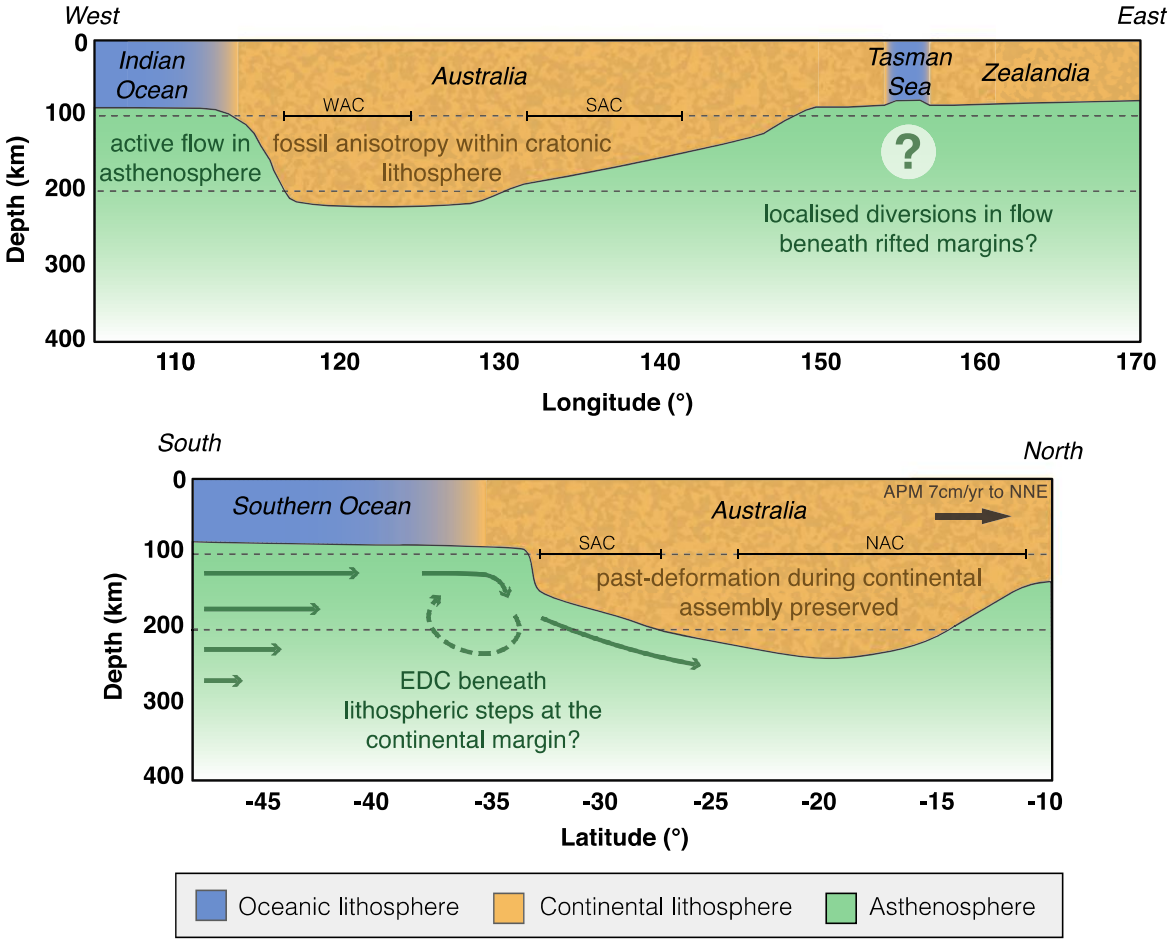

611

612

613 **Figure 5.** Pattern and sources of seismic anisotropy in the upper mantle as inferred from QL
614 scatterers. Deformational processes are illustrated via two generic cross-sections across the
615 Australian continent: (i) east-west profile (top), and (ii) north-south profile (bottom). The 100-
616 200 km zone of peak depth sensitivity for 100 second QL wave scattering is indicated by the
617 dashed horizontal lines. The topography and depth of the lithosphere-asthenosphere boundary is
618 based on profiles from AuSREM [41]. Abbreviations are as follows: APM- Absolute Plate Motion,
619 EDC- Edge Driven Convection, NAC- North Australian Craton, SAC- South Australian Craton,
620 WAC- West Australian Craton.

Figures

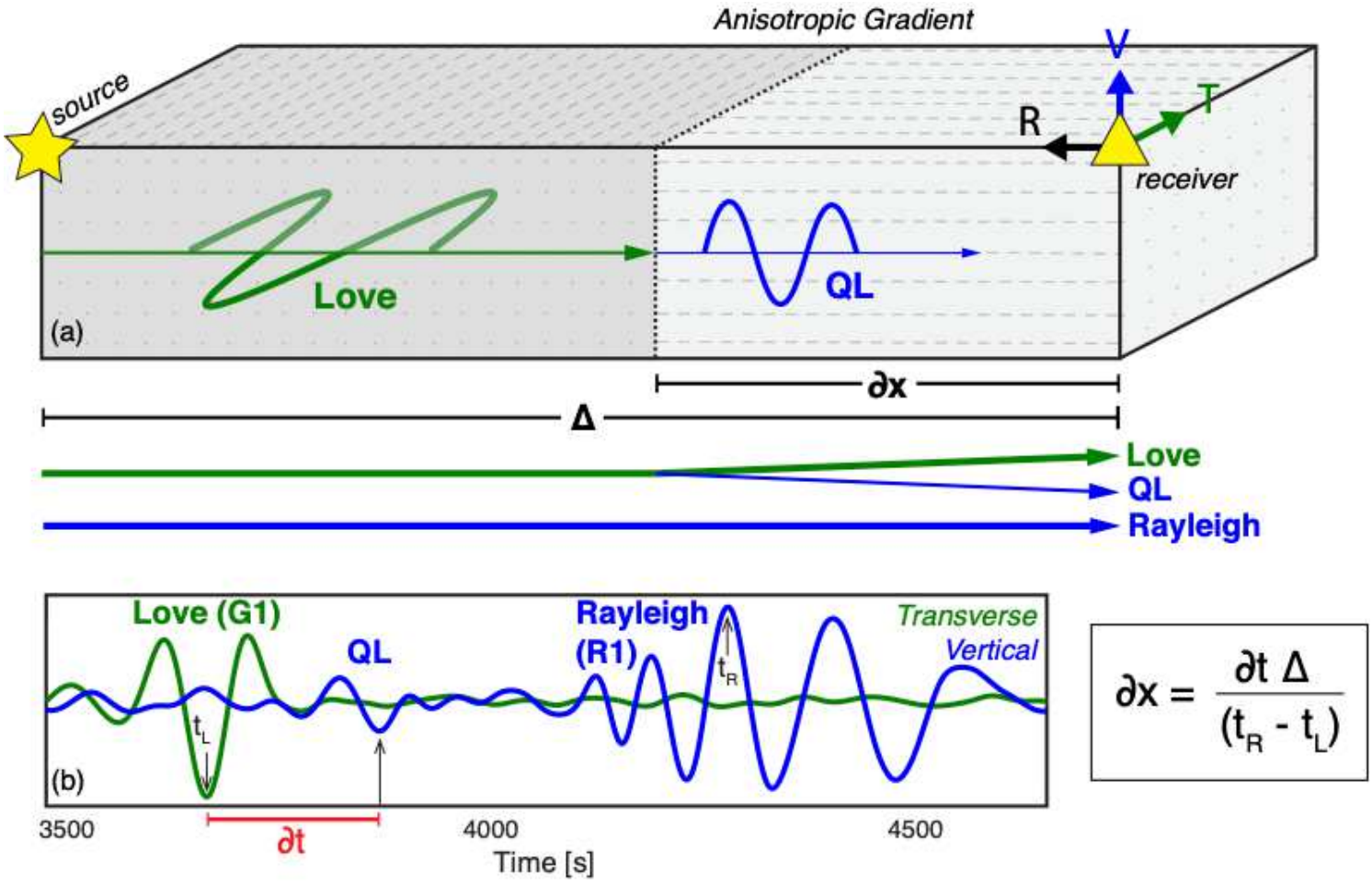

Figure 1

Process of QL wave scattering due to an anisotropic gradient. (a): Schematic illustration of a Love wave with transverse (T) particle motion (indicated in green), which upon encountering a lateral gradient in seismic anisotropy, partially converts into a QL wave with the same phase velocity and vertical (V) particle motion (indicated by blue) as a Rayleigh wave. The fundamental Love (G1) and Rayleigh (R1) waves travel a distance Δ between the source and receiver, whereas the QL wave only travels a distance δx between the scattering location and the receiver. The scattering is caused by a change in strength and/or orientation of the mantle anisotropy, indicated by the grey fabric pattern. (b): Example recording of a QL wave arrival that is found on the vertical component between G1 and R1. The distance to the scattering point (δx) is related to the time delay (δt) between the QL and G1 via the equation shown.

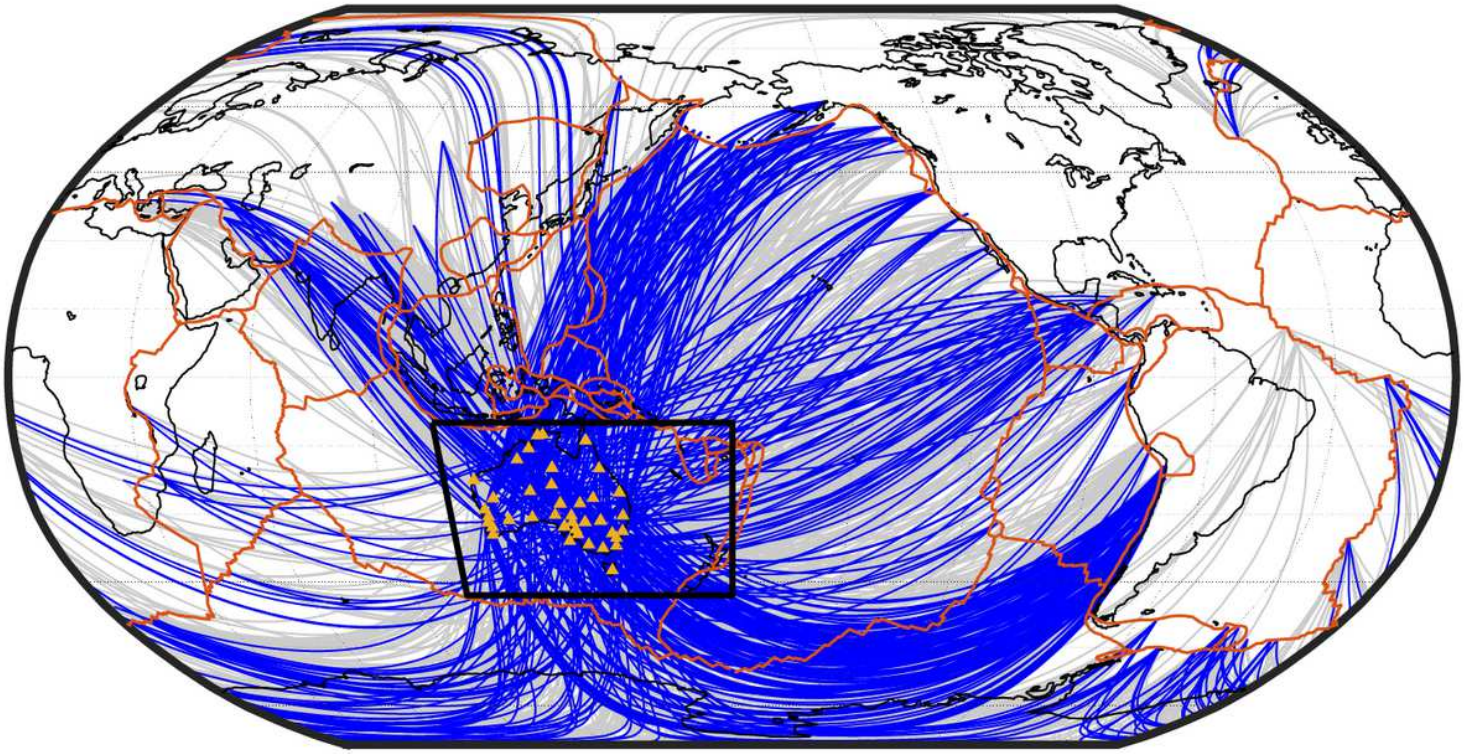

Figure 2

Global distribution of source-receiver paths analyzed for QL waves. Great-circle paths on which QL waves were present are shown in blue, the remainder in grey. The location ofanisotropic gradients within the area of interest (black box, Fig. 3) is investigated using 43 seismic receivers (yellow triangles) based within Australia. Plate boundaries (in orange) from 57.

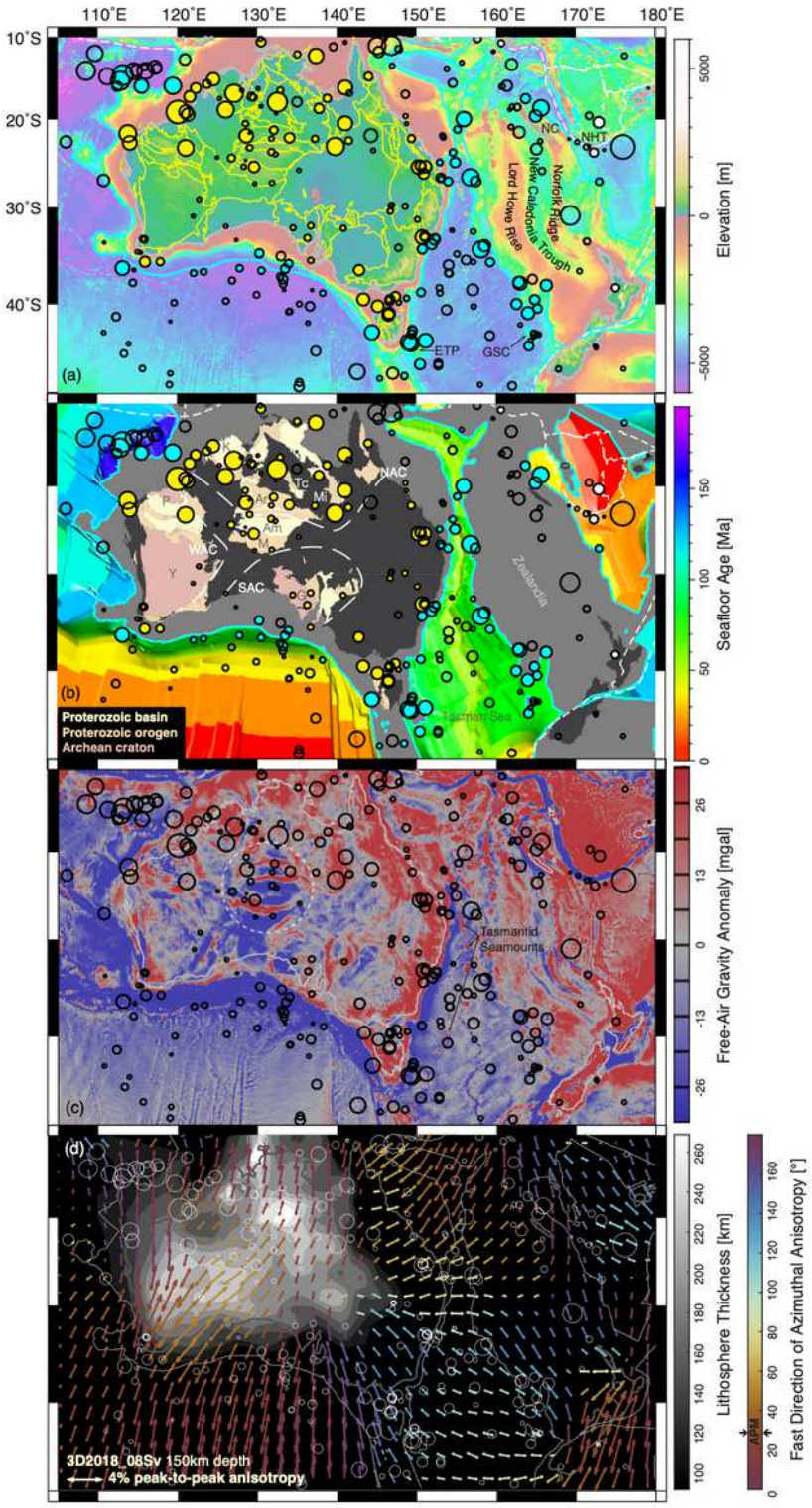

Figure 3

QL wave scattering points (black circles) compared to (a): surface topography 58, (b): seafloor age 28, the ocean-continent boundary, and the Precambrian tectonic elements ofAustralia 59, (c): free-air gravity 60, and (d): azimuthal anisotropy from 3D2018_08Sv 8 and thelithospheric thickness from AuSREM 31,41. Circles are scaled in size relative to the amplitude of the QL wave. Those which coincide (within a typical error of 100 km) with either a plate boundary (dashed white lines), the ocean-continent margin

(solid cyan lines), or geological provinces within Australia (yellow lines) 33, are highlighted by a solid circle with the respective color in (a) and (b). In (a) abbreviations are as follows: ETP- East Tasman Plateau, GSC- Gilbert Seamount Complex, NC- New Caledonia, NHT- New Hebrides Trench. In (b) abbreviations refer to major Precambrian provinces: Am- Amadeus, Ar- Arunta, G- Gawler, K- Kimberley, M- Musgrave, Mi- Mount Isa, P- Pilbara, Tc- Tennant Creek, Y- Yilgarn. White dashed lines show the approximate extent of the West Australian Craton (WAC), North Australian Craton (NAC), and South Australian Craton (SAC). In (c) the large dashed white circle over central Australia highlights the location of prominent E-W trending gravity anomalies. In (d) azimuthal anisotropy is illustrated by the arrows, with colors indicating the fast direction orientation, and the length of the arrow relative to the strength of anisotropy (refer to legend for scale).

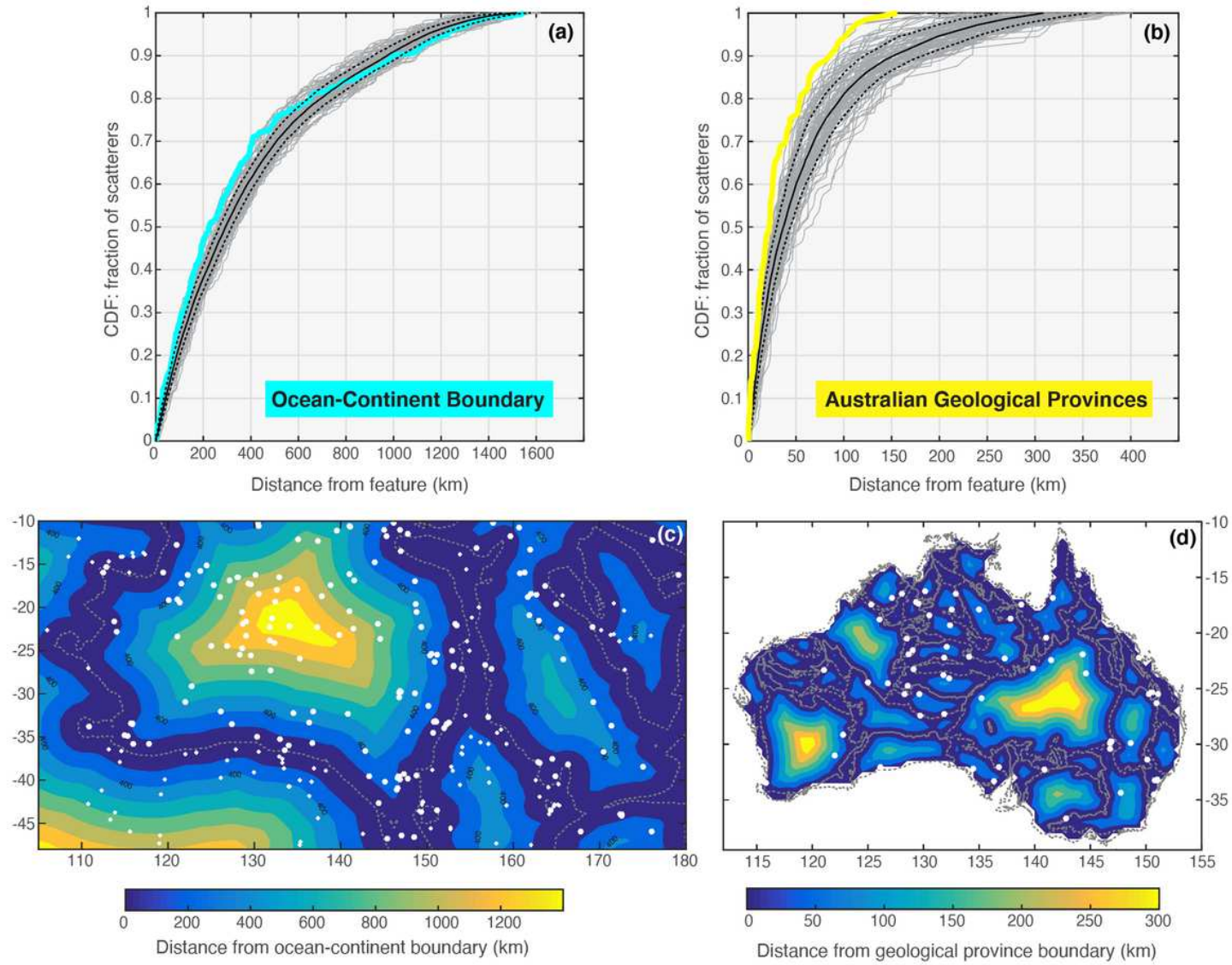

Figure 4

Distance of QL scatterers relative to associated features. (a-b): Cumulative distribution functions (CDF) showing the fraction of all observed QL scatters as a function of distance from the ocean-continent boundary 28 (cyan line) and major geological provinces (yellow line) 33. The same CDFs are generated

for 100 sets of the equivalent number of points randomly located across the study area (thin grey lines), alongside their mean (solid black line) and one standard deviation (dotted black line). (c-d) Maps showing spatial distribution of QL scatterers (small white symbols) compared to contours of the distance from either the ocean-continent boundary (c) or the geological province boundaries (d).

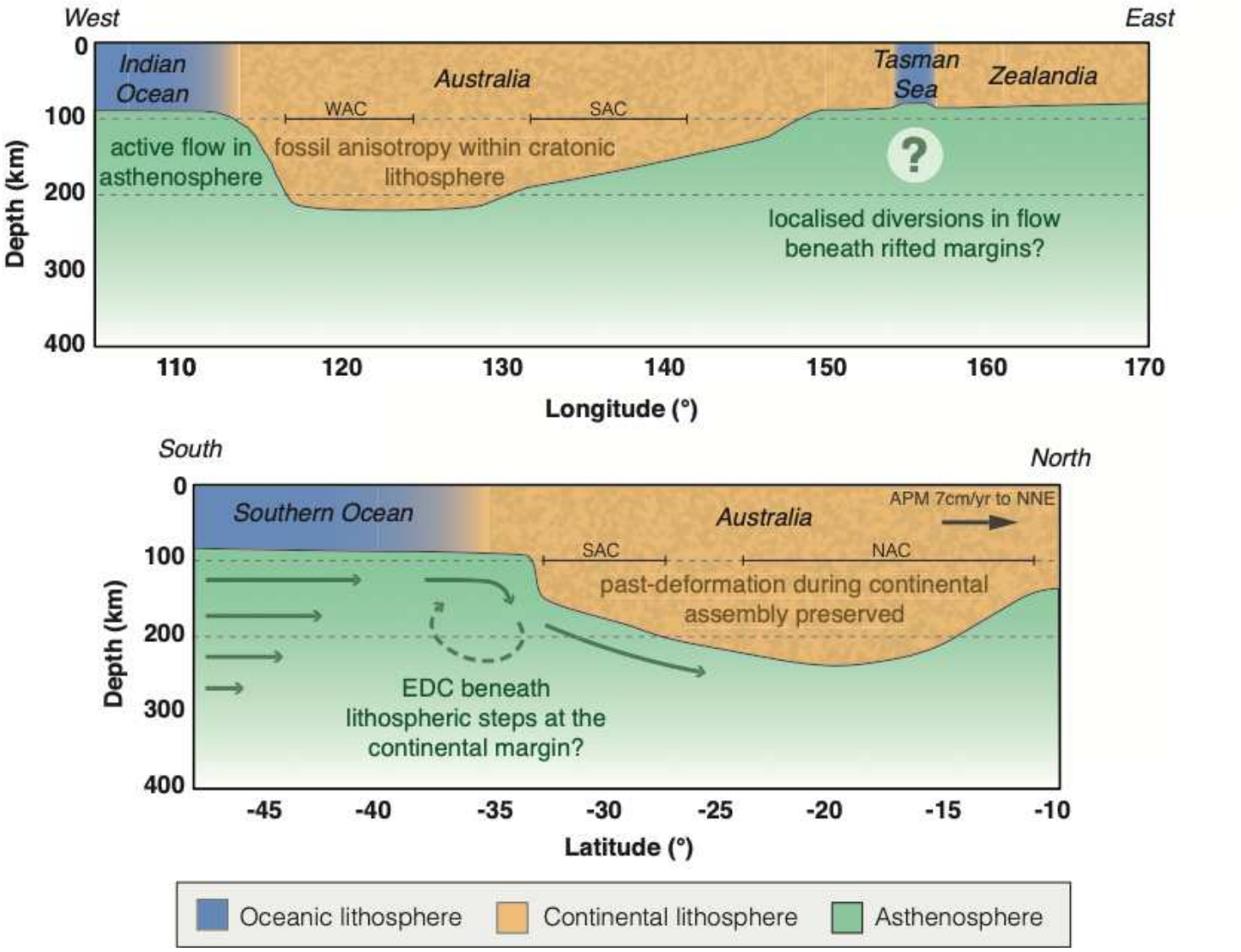

Figure 5

Pattern and sources of seismic anisotropy in the upper mantle as inferred from QL scatterers. Deformational processes are illustrated via two generic cross-sections across the Australian continent: (i) east-west profile (top), and (ii) north-south profile (bottom). The 100-200 km zone of peak depth sensitivity for 100 second QL wave scattering is indicated by the dashed horizontal lines. The topography and depth of the lithosphere-asthenosphere boundary is based on profiles from AuSREM 41. Abbreviations are as follows: APM- Absolute Plate Motion, EDC- Edge Driven Convection, NAC- North Australian Craton, SAC- South Australian Craton, WAC- West Australian Craton.

Supplementary Files

This is a list of supplementary files associated with this preprint. Click to download.

- SupplementaryInformationClean.pdf
- TableS1.xlsx